Thermomechanical analysis of carbon fiber-reinforced polymer representative volume elements with voids

(Article begins on next page)

22 November 2024

Thermomechanical analysis of CFRP representative volume elements with voids

M. Petrolo, A. Pagani, M. Trombini, R. Masia, E. Carrera

MUL² Lab, Department of Mechanical and Aerospace Engineering, Politecnico di Torino,
Corso Duca degli Abruzzi 24, 10129 Torino, Italy

Author for correspondence:
Marco Petrolo
MUL² Lab, Department of Mechanical and Aerospace Engineering,
Politecnico di Torino,
Corso Duca degli Abruzzi 24,
10129 Torino, Italy,
tel: +39 011 090 6845,
e-mail: marco.petrolo@polito.it

Abstract

The present work presents results of numerical simulations to investigate the effect of different void percentages on composite materials' coefficient of thermal expansion (CTE) and local stress fields. A random distribution of voids is considered within the Representative Volume Element (RVE) matrix, and different types of microstructures are considered, including square-packed and randomly distributed fibers. The use of a higher-order beam model within the framework of Carrera Unified Formulation (CUF) leads to a Component Wise (CW) approach, resulting in an accurate, 3D description of the cross-section although using a 1D formulation. Numerical results for different fiber volume fractions and void concentration percentages demonstrate the agreement of the computed effective coefficients of thermal expansion of the present micromechanical thermoelastic model with references from the literature. The local stress fields is affected by voids, with higher effects over the matrix. Furthermore, higher void fractions lead to higher variability of stress peaks.

Keywords: Micromechanics; Voids; CUF; RVE; Composite materials; Statistical analysis

1 Introduction

Fiber-reinforced composites have excellent thermomechanical properties, such as lightweight, high-temperature mechanical performances and good thermal stability. A fundamental factor governing the thermal behavior of composite materials is the coefficient of thermal expansion (CTE), which describes the material's tendency to expand or contract when subjected to changes in temperature. CTE plays a critical role in designing composite materials since it can directly determine the dimensional stability of the structure and thermal stress distribution. Furthermore, the multiscale nature of composite materials, with their complex hierarchical structures, may influence CTE, and multiscale models are desirable for accurate predictions. These models must capture the behavior of the constituent materials at the microscale while also accounting for the macroscopic response of the composite as a whole.

Another crucial aspect is the growth of defects that inevitably occur during the manufacturing process. Specifically, voids are primary manufacturing defects that significantly influence thermoelastic properties. The presence of voids introduces regions of reduced stiffness and altered stress distributions within the material, thereby affecting its overall thermomechanical behavior. Understanding the influence of voids on thermoelastic properties is of paramount importance [1]. Little et al. [2] compared the use of micro-computed thermography (micro-CT) to different conventional techniques [3, 4] for identifying the size, shape, and distribution of voids in carbon fiber reinforced composite (CFRC). More recently, the X-ray Computed Tomography [5] was adopted as the framework for measuring voids in composites. Air gaps are often present in 3D printed fiber reinforced composites [6], where void content is higher in 0° printing direction [7] and have an impact on mechanical performance [8]. Unidirectional laminates demonstrated higher voids sensitivity than the fabric laminates [9], while some experimental programs investigated the impact of void content on static strength, fatigue life, and interlaminar shear strength (ILSS) [10, 11, 12]. Additionally, an optimized cure cycle can decrease void volume fraction, thus improving the mechanical properties of composites [13, 14]. Furthermore, voids are crucial in the formation process of crack propagation [15, 16, 17].

Computational micromechanics emerged as an approach for investigating defects at a microscale level. Micromechanics enables retrieving the homogenized thermomechanical properties and the local stress and strain fields via dehomogenization. Numerous analytical techniques have been developed, offering more sophisticated solutions for analyzing composite materials. One notable example is the Method of Unit Cells (MOC) [18], which has been widely used to study composites' mechanical and thermal behavior. In addition to MOC, more recent advancements include the Generalized Method of Cells (GMC) [19, 20] and the High-Fidelity Generalized Method of Cells (HFGMC) [21]. These methods have further refined the analysis of composite materials by considering additional factors such as material heterogeneity, interface properties, and the presence of defects. Most of these methods and numerical simulations for the homogenization analysis usually employ Representative Volume Element (RVE) models [22, 23, 24], which represent the smallest geometric entity containing all the information about material properties and volume fraction of the constituents. Recently, numerical simulations

have been conducted employing commercials such as Abaqus [25]. Another recently popular method for carrying out numerical homogenization and dehomogenization analyses is represented by the Mechanics of Structure Genome (MSG) [26], based on the Variational Asymptotic Method (VAM) [27]. The Finite Element Method (FEM) represents a viable approach to studying micromechanics. Various research studies have utilized FEM to model the microscale through the use of RVE [28, 29, 30, 31, 32], while many works embedded voids into FEM to retrieve elastic properties of composites [33, 34, 35, 36, 37]. Regarding the thermoelastic framework, MSG-based finite element analysis was adopted to compute the CTE of solid models [38], while Wei et al. [39] studied the influence of voids on homogenized CTE using a 3D Abaqus formulation.

The computational cost of 3D FEM analyses can be heavy when dealing with 3D RVE or nonlinear cases. Employing the Carrera Unified Formulation (CUF) [40] reduces the computational cost, thus maintaining high accuracy of results. Previous micromechanics investigations [41, 42] demonstrated the advantages of using CUF compared to classical formulations. In the work of Sánchez-Majano [43], MSG coupled with CUF for the computation of thermoelastic properties of a Repeatable Unit Cell (RUC) model. The influence of void has been investigated on the linear response of composite [44], and other works retrieve the local stress and strain fields using a statistical approach [45, 46].

The present work aims to extend CUF micromechanics to a thermoelastic framework for retrieving the homogenized CTE and the local stress distributions with a novel computationally efficient technique. Moreover, the investigation focuses on the effect of random voids on the homogenized thermoelastic properties, using statistical analysis to analyze the impact of void distributions at a given void volume fraction, which is rarely mentioned and investigated in the literature. An additional advantage of the current methodology lies in its capacity to easily model diverse RVE architectures, owing to the utilization of a higher-order formulation that enables accurate geometrical and material modeling within a one-dimensional kinematic model. Finally, the local stress fields over RVE's fiber and matrix with voids are computed. The work is organized as follows: Section 2 presents the high-order theory formulation; Section 3 introduces the micromechanics model; Section 4 presents an overview of the statistical investigation; Section 5 provides numerical results; and their discussion is underlined in Section 6. Finally, the conclusions are given in Section 7.

2 Structural theories and FEM

A refined structural model is essential when dealing with complex mechanical behaviors, such as the deformation field that occurs across the cross-section of an RVE; the present work exploits the capabilities of a refined 1D kinematic model based on the CUF. In Eq. (1), the three components of the displacement field are defined according to the reference system in Fig. 1,

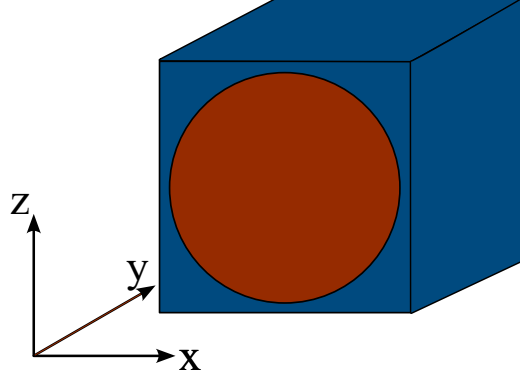$$\boldsymbol{u}(x, y, z) = \{u_x \ \ u_y \ \ u_z\} \tag{1}$$

Figure 1 Square-packed RVE model and reference frame.

In CUF [40], the displacement field is defined as in Eq. (2),

$$\boldsymbol{u}(x,y,z) = F_\tau(x,z)\boldsymbol{u}_\tau(y) \qquad \tau = 1,2,...,M \tag{2}$$

where $F_\tau(x,z)$ are the expansion functions employed over the cross-section, $\boldsymbol{u}_\tau(y)$ is the vector of general displacements, and M is the number of terms in the expansion. In addition, τ denotes the summation of the expansion terms. Arbitrary polynomials can be selected as 2D expansion functions. This paper employs Lagrange polynomials, thereby enabling a Component-Wise (CW) approach in which fibers and matrix are described with different sets of primary variables. In the present work, 9-node bi-quadratic expansion elements (L9) are employed to discretize the model cross-section. Equation (3) shows the displacement field for L9,

$$
\begin{aligned}
u_x &= F_1 u_{x1} + F_2 u_{x2} + F_3 u_{x3} + ... + F_9 u_{x9} \\
u_y &= F_1 u_{y1} + F_2 u_{y2} + F_3 u_{y3} + ... + F_9 u_{y9} \\
u_z &= F_1 u_{z1} + F_2 u_{z2} + F_3 u_{z3} + ... + F_9 u_{z9}
\end{aligned}
\tag{3}
$$

where $u_{n1},...,u_{n9}$ are the translational displacement components related to each node of the element. By modeling the longitudinal direction through standard 1D FEM terms, the shape functions are introduced in Eq. (4):

$$\boldsymbol{u}(x,y,z) = F_\tau(x,z)N_i(y)\boldsymbol{u}_{\tau i} \qquad \tau = 1,2,...,M \qquad i = 1,2,...,p+1 \tag{4}$$

where $N_i(y)$ represents the shape functions of p-th order, $\boldsymbol{u}_{\tau i}$ is the vector of nodal displacements, and M stands for the number of expansion terms. Equation (5) defines the stress,

$$\boldsymbol{\sigma}^T = \{\sigma_{xx} \ \ \sigma_{yy} \ \ \sigma_{zz} \ \ \sigma_{xy} \ \ \sigma_{xz} \ \ \sigma_{yz}\} \tag{5}$$

The geometrical equation, see Eq. (6), defines the relation between strains and displacements:

$$\boldsymbol{\varepsilon} = \boldsymbol{D}\boldsymbol{u} \tag{6}$$

where $\boldsymbol{D}$ is the 6×3 differential operator. Moreover, the use of Hooke's law, Eq. (7), enables the establishment of a relationship between stress and strain:

$$\boldsymbol{\sigma} = \boldsymbol{C}\boldsymbol{\varepsilon} \tag{7}$$

where $\boldsymbol{C}$ is the stiffness matrix of the material. The governing equations are derived based on the Principles of Virtual Displacement (PVD). In the context of static analysis, the PVD can be expressed as in Eq. (8):

$$\delta L_{int} = \delta L_{ext} \tag{8}$$

where δL_{int} is the strain energy and δL_{ext} is the work of the external forces. While δ is used to indicate the virtual variation of the quantity. As shown in [40], the strain energy can be formulated as in Eq. (9):

$$\delta L_{int} = \delta \boldsymbol{u}_{sj}^T \boldsymbol{k}_{ij\tau s} \boldsymbol{u}_{\tau i} \tag{9}$$

where the explicit form of the 3×3 Fundamental Nucleus (FN) $\boldsymbol{k}_{ij\tau s}$ is expressed in Eq. (10):

$$\boldsymbol{k}_{ij\tau s} = \int_V F_s(x,z) N_j(y) \boldsymbol{D}^T \boldsymbol{C} \boldsymbol{D} F_\tau(x,z) N_i(y) dV \tag{10}$$

Equation (11) defines the external load,

$$\delta L_{ext} = \delta \boldsymbol{u}_{sj}^T \boldsymbol{P}_{sj} \tag{11}$$

where $\boldsymbol{P}_{sj}$ is the 3×1 external load vector and is referred to as the FN of the load vector. The global stiffness matrix and the external load vector are assembled by iterating the indices i,j,τ,s. The first two indexes, i,j, denote the loop on the FEM nodes, while τ,s are the loop indices on the cross-section nodes.

3 Micromechanics formulation

One of the aims of the present study is to evaluate the effective thermoelastic properties of composite materials, particularly the Coefficient of Thermal Expansion, through a micromechanical analysis. Periodic Boundary Conditions (PBC) are applied in the micromechanics framework to ensure that opposite boundary surfaces undergo the same deformation mode [33, 47]. Figure 2 describes the reference frame adopted for the description of the micromechanical model and the application of PBC, expressed in Eq. (12):

$$u_i^{j+}(x,y,z) - u_i^{j-}(x,y,z) = \bar{\varepsilon}_{ik}\Delta x_k^j \qquad\qquad \Delta x_k^j = x_k^{j+} - x_k^{j-} \tag{12}$$

where j+ and j- indicate the positive and negative directions of the x_k and $\bar{\varepsilon}_{ik}$ is the macroscopic strain vector. The cross-section of the 1D models is discretized with nine-node bi-quadratic elements (L9), whereas along the fiber direction, four-node cubic elements (B4) are employed.
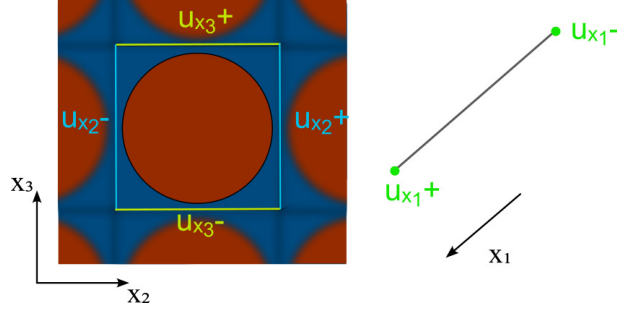
Figure 2 Reference frame for micromechanics and PBC.

The thermoelastic analysis considers the stress field given both from the elastic and thermal contributions, as illustrated in Eq. (13),

$$\sigma_{ij} = \sigma_{ij}^E + \sigma_{ij}^T \tag{13}$$

where E stands for elastic and T thermal. The present homogenization procedure first involves the resolution of the static problem in order to obtain the effective stiffness matrix, which is then employed in the effective CTE vector. In the micromechanics framework, the local solutions, such as the strain and stress vectors, have an average value over the RVE volume. The local elastic stress field σ_{ij}^E is defined in Eq. (7), and its macroscopic value $\bar{\sigma}_{ij}^E$ [48] is expressed in Eq. (14):

$$\bar{\sigma}_{ij}^E = \frac{1}{V} \int_V \sigma_{ij}^E dV \tag{14}$$

in the same way, Eq. (15) defines the macroscopic strain vector,

$$\bar{\varepsilon}_{ij}^E = \frac{1}{V} \int_V \varepsilon_{ij}^E dV \tag{15}$$

Then, the effective elastic coefficients matrix $\bar{C}_{ijkl}$ can be easily retrieved from Eq. (16),

$$\bar{\sigma}_{ij}^E = \bar{C}_{ijkl} \bar{\varepsilon}_{ij}^E \tag{16}$$

Moreover, Eq. (17) represents the local stress field given by the thermal contribution due to the application of a temperature variation θ:

$$\sigma_{ij}^T = \beta_{ij} \theta \tag{17}$$

where $\beta_{ij} = -C_{ijkl} \alpha_{ij}$ is the local thermal-induced stress vector. Note that the temperature field applied to the RVE, unlike the stress and strain, is considered to be uniform throughout the heterogeneous material. By applying the integral over the volume of the thermal stress vector, it is possible to find the homogenized value σ_{ij} as in Eq. (14). Then, by obtaining Eq. (17) for $\bar{\beta}_{ij}$ and exploiting the relationship between $\bar{\beta}_{ij}$ $\bar{\alpha}_{ij}$ and $\bar{\beta}_{ij}$, the effective CTE vector can be obtained by Eq. (18):

$$\bar{\sigma}_{ij}^T = -\bar{C}_{ijkl} \bar{\alpha}_{ij} \theta \tag{18}$$
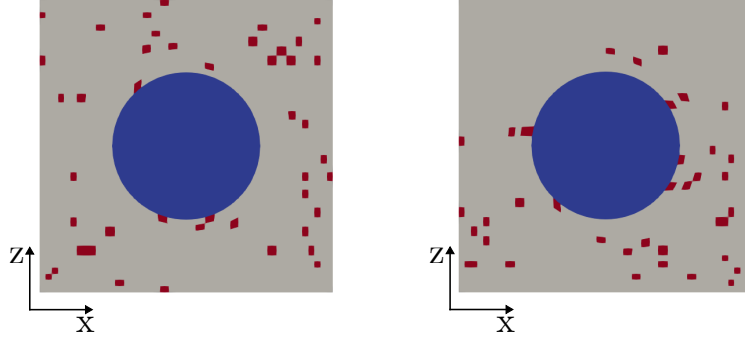
7

Figure 3 Two different sets of 3% of void content over the matrix of a square-packed RVE.

More details about the elastic CUF micromechanics framework are available in [41, 42]. To model voids, a technique previously employed in [44, 45, 46] is used, where a set of Gauss points within the matrix domain is randomly selected and assigned low elastic moduli. The FE matrices computation uses Gauss-Legendre quadrature, and the integrals involving voids' Gauss points are evaluated with modified elastic moduli. To achieve a desired void volume fraction, matrix Gauss points are randomly chosen as void sites. This process generates voids with a domain size corresponding to the volume associated with the selected Gauss point rather than the entire element. Different combinations of Gauss points can produce the same total void volume fraction. During the FE matrices computation, void sites' Gauss points are considered to have negligible elastic properties. Whilst regarding the thermal behavior, voids are associated with the CTE of the air, equal to 10^{-3} K^{-1}. An example of different Gauss point selections in a square-packed RVE with a 3% void volume fraction is shown in Fig. 3.

4 Statistical analysis

The novelty proposed in this article involves the extension of the effect of voids on the thermomechanical response of composites. One hundred defect distributions were randomly generated for each void volume fraction. In the pure-elastic related study by Carrera et al. [44], 100 random distributions were used for each percentage, and the same number was considered for the present investigation, also to satisfy the need for a reliable statistical analysis. The absolute maximum and minimum of each mechanical quantity for each distribution of results were considered. Furthermore, the mean value and standard deviation s, Eq. (19), were taken into account:

$$s = \sqrt{\frac{1}{100 - 1} \sum_{i=1}^{100} (x_i - \bar{x})^2} \tag{19}$$

x_i is a given thermomechanical property and $\bar{x}$ is the mean value of each distribution. Also, the analysis considered the first, second, and third quartiles - q_1, q_2, and q_3. The first quartile is a statistical measure that partitions a given dataset into two parts, such that 25% of the data values are located to the left of the first

quartile, and 75% is located to the right. Conversely, the third quartile partitions the dataset in such a way that 75% of the data values are located to the left of the third quartile, and 25% is located to the right [49]; q_2 is also known as the median. A visual representation of statistical parameters was employed using boxplots and probability density functions [50]. These graphical tools allow observation of quartiles, notch extremes, and outliers, providing a clear view of the data distribution [51]. The notch extremes represent interval endpoints, and they are computed as shown in Eq. (20):

$$q_L = q_2 - 1.57 \frac{q_3 - q_1}{\sqrt{100}}, \quad q_U = q_2 + 1.57 \frac{q_3 - q_1}{\sqrt{100}} \tag{20}$$

q_L and q_U are the lower and the upper endpoints. The outliers, see Eq. (21), are defined as the values exceeding the endpoints,

$$q < q_L \quad \& \quad q > q_U \tag{21}$$

5 Numerical results

The first numerical case aims to assess the present approach - CUF-Micromechanics (CUF-MCM) - using benchmarks from the literature for a square-packed RVE without defects. Furthermore, the variation of the effective CTE due to growing void fractions is investigated. In the second part of the numerical results, the stress and strain fields within the RVE resulting from thermomechanical loads are assessed using dehomogenization. Initially, the outcomes obtained without voids are compared with reference values. The subsequent analysis focuses on the changes in the stress distribution when voids are introduced.

5.1 Verification of the thermoelastic micromechanical analysis

The square-packed RVE, depicted in Fig. 1, is the selected architecture for the verification phase. First, pristine RVE are considered with increasing fiber volume fractions. The material properties of the constituents of the square-packed RVE are listed in Table 1. The mesh has 172 L9 + 2 B4 elements, leading to 20412 degrees of freedom (DOF), and the same discretization is adopted for each fiber volume fraction. Figure 4 shows the cross-section discretization and the elements along the y-direction for the RVE with 64% of fiber volume fraction. The present higher-order CUF 1D simulation (CUF-MCM) is compared to (i) HFGMC method [21]; (ii) MSG-based analysis with solid elements [38]; (iii) MSG coupled with CUF [43].

Figure 5 illustrates the longitudinal and transversal CTE as a function of the fiber volume fraction, whereas the results for the 64% of fiber volume fraction case are listed in Table 2.

Table 1 Thermoelastic properties of the constituents for the Carbon/Epoxy composite [38].

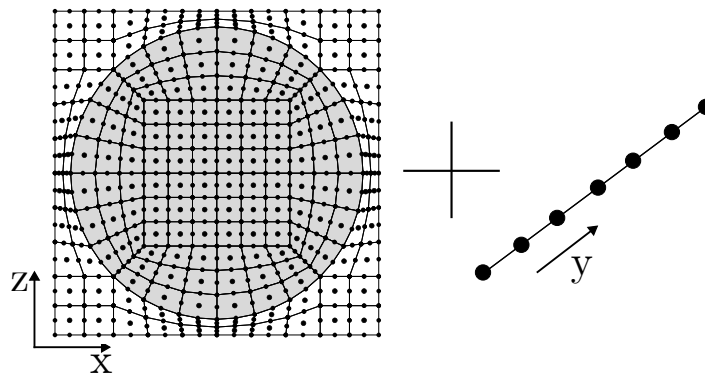|	T300 carbon fiber		Epoxy resin matrix
E_{11} [GPa]	230.00	E [GPa]	3.45
$E_{22} = E_{33}$ [GPa]	40.00	ν [-]	0.35
$G_{12} = G_{13}$ [GPa]	24.00	$\alpha \times 10^6$ [K^{-1}]	63.00
G_{23} [GPa]	14.30	κ [Wm^{-1}K^{-1}]	0.20
$\nu_{12} = \nu_{13}$ [-]	0.26		
ν_{23} [-]	0.40		
$\alpha_{11} \times 10^6$ [K^{-1}]	-0.70		
$\alpha_{22} = \alpha_{33} \times 10^6$ [K^{-1}]	10.00		
$\kappa_{11} = \kappa_{22} = \kappa_{33}$ [Wm^{-1}K^{-1}]	129.00		

Figure 4 Discretization for the square-packed 64% V_f RVE with 172 L9 elements for the cross-section and 2 B4 elements along y-direction.

Table 2 Homogenized longitudinal and transversal CTE for the square-packed RVE with 64% of fiber volume fraction, compared with literature results.

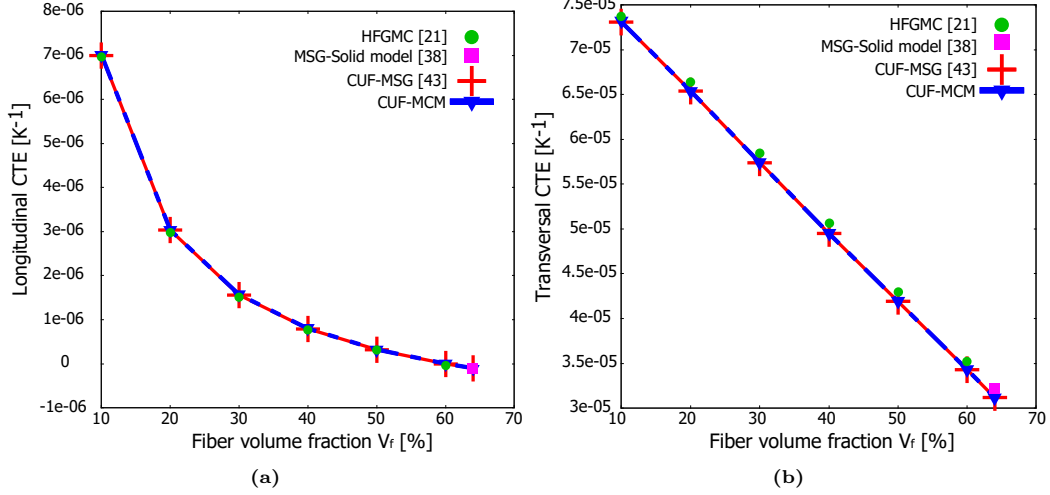| Model	$\alpha_{11} \times 10^6$ [K^{-1}]	$\alpha_{22} = \alpha_{33} \times 10^6$ [K^{-1}]
HFGMC [21]	-0.109	32.033
MSG-solid model [38]	-0.108	31.975
CUF-MSG [43]	-0.102	31.161
CUF-MCM	-0.096	31.169

Figure 5 Longitudinal and transversal CTE for the square-packed RVE for increasing volume fractions.

In addition, the relative percentage deviation between the current analysis and the reference [43] is computed as in Eq. (22):

$$E[\%] = \frac{\left(\alpha_{ii}^{CUF-MCM} - \alpha_{ii}^{CUF-MSG}\right)}{\alpha_{ii,max}^{HFGMC}} \times 100 \tag{22}$$

where $\left(\alpha_{ii}^{CUF-MCM} - \alpha_{ii}^{CUF-MSG}\right)$ are the two sets of CTE to be compared for each fiber volume fraction V_f^j; $\alpha_{ii,max}^{HFGMC}$ is the maximum value of CTE obtained at 10% of fiber volume fraction. Table 3 presents the percentage deviations computed using Eq. (22).

The analysis of the results suggests a perfect match between the present and the other methods considered. Only the transversal CTE α_{22} along the x-direction is reported since it coincides with that obtained along the z-direction.

Table 3 Relative deviation between the present analysis and CUF-MSG [43], referred to the corresponding HFGMC solution [21], for the square-packed RVE with different fiber volume fractions.

	Fiber volume fraction [%]					
	10	20	30	40	50	60
Relative deviation $E[\%]$	Ref HFGMC $\alpha_{11,max}^{HFGMC} = 6.97 \times 10^{-6}$ [K^{-1}]					
	0.182	0.103	0.074	0.059	0.052	0.045
	Ref HFGMC $\alpha_{22,max}^{HFGMC} = 7.37 \times 10^{-5}$ [K^{-1}]					
	0.001	0.020	0.035	0.045	0.055	0.041

5.2 Influence of fiber volume fraction and voids on CTE

The RVE model employed for the current assessment is based on the work of Wei et al. [39], and two values of fiber volume fraction are evaluated: 57% (see Fig. 6a) and 80% (see Fig. 6b). The 57% V_f RVE has a 9.96×9.96×9.96 μm cubic shape, whereas the 80% V_f RVE is 8.40x8.40x8.40 μm. The material is a C/C composite, and the CTE of the orthotropic fiber and the isotropic matrix are listed in Table 4. According to [52], the current RVE is not a proper hexagonal-packed RVE but is considered a hexagonal bundle enforced in a square cross-section shape. The void content ranges from 2 to 8%, and the homogenized CTE is compared with [39], where 3D Abaqus finite elements equal to 43725 for the 57% RVE and 43680 for the 80% case were used. Figure 7a shows the 57% V_f RVE with 6% of voids, whereas the 2% of void content is in Fig. 7b for the 80% V_f RVE. A convergence analysis is first carried out on the 57% V_f RVE and shown in Fig. 8. The horizontal axis reports the CUF numerical models with increasing cross-sectional elements. In contrast, the vertical axis represents the percentage deviation of the CTE for the given mesh and is computed using the most refined model as the reference, 1000 L9 + 2 B4. According to the convergence analysis, the model with 160 L9 and 2 B4 elements, resulting in 19740 DOF, exhibits a deviation of 0.0028% and is thus adopted for the following analyses. For the 80% case, 23996 DOF are employed, and the mesh chosen has 200 L9 + 2 B4 elements, as shown in Figs. 9a and 9b.
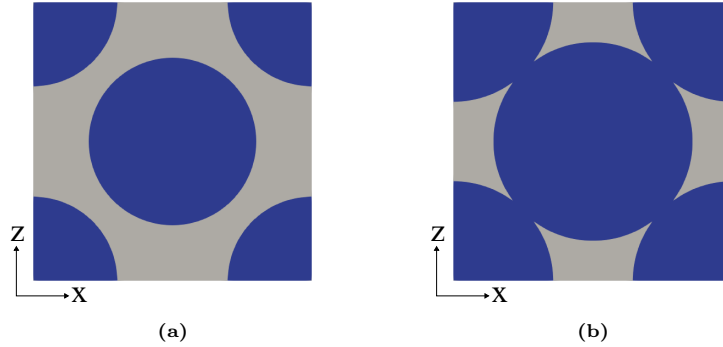

(a)   (b)

Figure 6 Cross-section of RVE with (a) 57% and (b) 80% fiber volume fraction without voids.

Table 4 Thermoelastic properties of the constituents for the C/C composite [39].

	Carbon fiber		Carbon matrix
E_{11} [GPa]	350.00	E [GPa]	10.25
$E_{22} = E_{33}$* [GPa]	13.80	ν [-]	0.23
$G_{12} = G_{13}$* [GPa]	9.00	$\alpha \times 10^6$ [K^{-1}]	4.00
G_{23} [GPa]	4.80		
$\nu_{12} = \nu_{13}$ [-]	0.2		
ν_{23}* [-]	0.3		
$\alpha_{11} \times 10^6$ [K^{-1}]	-1.00		
$\alpha_{22} = \alpha_{33} \times 10^6$ [K^{-1}]	18.00		

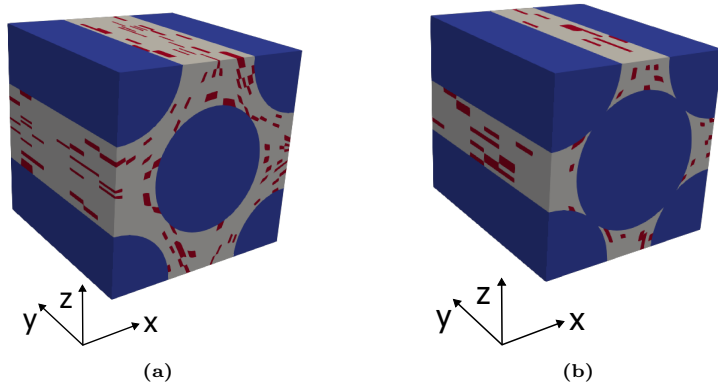*properties assumed as they were not indicated

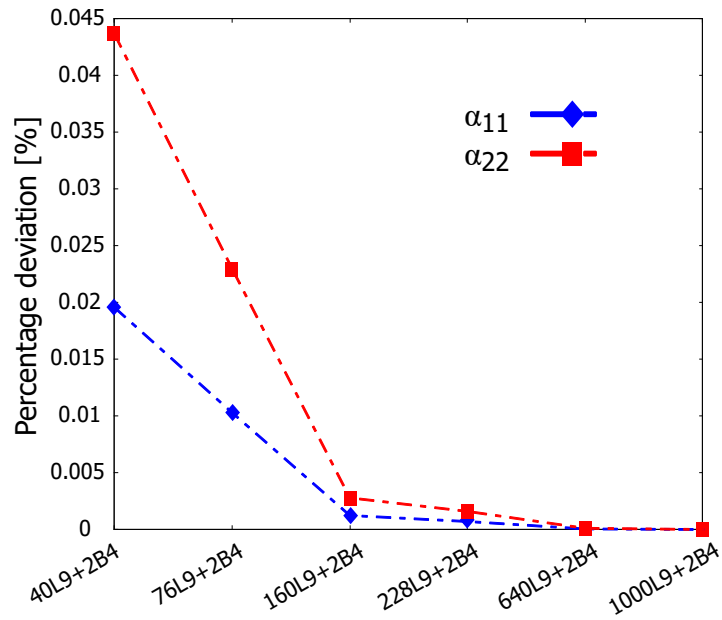Figure 7 RVE with (a) 57% V_f with 6% voids and (b) 80% V_f with 2% voids.

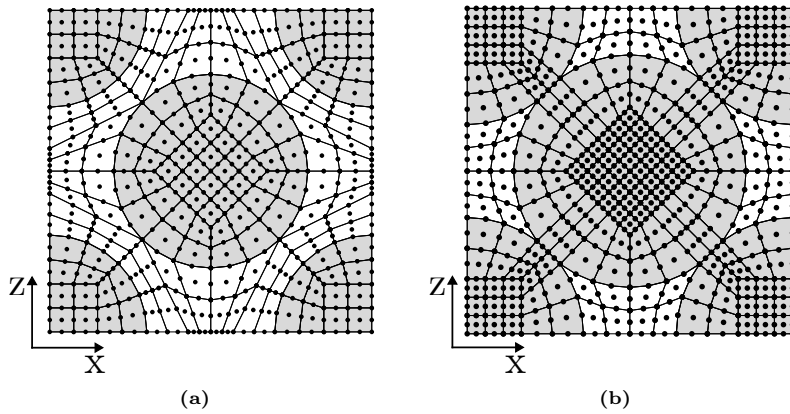Figure 8 Convergence analysis of the longitudinal and transversal CTE for the RVE with V_f=57%.

Figure 9 Cross-section discretizations for (a) V_f= 57% RVE with 160 L9 + 2 B4, and (b) V_f= 80% RVE with 200 L9 + 2 B4.

13

Table 5 Effective CTE of models with 57% and 80% of fiber volume fractions and no void content.

Model	$\alpha_{11} \times 10^6$ [K^{-1}]	$\alpha_{22} = \alpha_{33} \times 10^6$ [K^{-1}]
	V_f=57%	
3D Abaqus model [39]	-0.900	12.720
CUF-MCM	-0.909	13.082
	V_f=80%	
3D Abaqus model [39]	-0.962	16.450
CUF-MCM	-0.972	15.820

Table 6 Mean values of CTE obtained using CUF micromechanics and 3D Abaqus model [39] with increasing void volume fraction.

Void content	$\alpha_{11} \times 10^6$ [K^{-1}]		$\alpha_{22} = \alpha_{33} \times 10^6$ [K^{-1}]	
	CUF-MCM	3D Abaqus model [39]	CUF-MCM	3D Abaqus model [39]
		$V_f = 57\%$		
2%	-0.914	-0.920	13.247	12.800
4%	-0.918	-0.960	13.418	12.910
6%	-0.923	-0.980	13.596	13.010
8%	-0.927	-1.020	13.781	13.120
		$V_f = 80\%$		
2%	-0.975	-0.970	16.036	16.560
4%	-0.978	-0.980	16.261	16.780
6%	-0.980	-0.990	16.494	17.010
8%	-0.983	-1.020	16.737	17.270

Table 5 compares the homogenized CTE with the reference [39] for both cases of fiber volume fractions without voids, while Table 6 shows the comparison in the case of increasing void content. The statistical parameters for the 57% V_f RVE are in Table 7.

The results suggest that:

- In the case of the RVE without voids, the CUF has good accuracy in the computation of both the longitudinal and the transversal CTE. The inconsistencies with the reference values may be due to the different micromechanical frameworks and become more pronounced with larger void contents. Furthermore, some of the input properties for CUF were assumed as they were not indicated in the papers from the literature.

- Increasing void content leads to a decrease in the longitudinal CTE, whereas transversal CTE exhibits an increasing trend consistent with the reference values.

Table 7 Statistical parameters of homogenized CTE (K^{-1}) for the 57% V_f RVE.

	$\bar{x}$	s	min	max	q$_1$	q$_2$	q$_3$	Voids [%]
	-9.137	0.001	-9.138	-9.136	-9.137	-9.137	-9.136	2
$\alpha_{11} \times 10^7$	-9.181	0.001	-9.183	-9.180	-9.182	-9.181	-9.181	4
	-9.226	0.001	-9.228	-9.223	-9.226	-9.226	-9.225	6
	-9.270	0.001	-9.272	-9.268	-9.271	-9.270	-9.270	8
	13.247	0.002	13.241	13.252	13.246	13.247	13.248	2
$\alpha_{22} \times 10^6$	13.418	0.003	13.412	13.425	13.415	13.418	13.420	4
	13.596	0.004	13.586	13.606	13.593	13.596	13.598	6
	13.781	0.004	13.770	13.792	13.778	13.780	13.783	8

- By observing the standard deviation of CTE, the range of variability of properties is small. Consequently, voids affect the homogenized thermoelastic properties, but the void distribution over the matrix does not significantly affect the CTE.

5.3 Local stress fields

This section aims to investigate voids' effect on the local stress distribution. The first part of the section verifies the micromechanical model for obtaining the local stress distribution in the case without voids. The model used for the verification is a square-packed RVE, see Fig. 1, which is a boron fiber embedded in an aluminum matrix denoted as B/Al with a 20% of fiber volume fraction. Both fiber and matrix constituents are modeled as isotropic, and the thermoelastic properties presented in Table 8 were retrieved from [43].

Table 8 Thermoelastic properties of the constituents for the B/Al composite [43].

	Boron fiber	Aluminum Matrix
E [GPa]	379.3	68.3
ν [-]	0.1	0.3
$\alpha \times 10^6$ [K^{-1}]	8.1	23.0
κ [Wm^{-1}K^{-1}]	27.4	237.0

The discretization consists of 176 L9 for the cross-section, whereas 2 B4 act along the y-direction, as shown in Fig. 10, resulting in 21084 DOF. The mesh was chosen due to a convergence analysis on the homogenized thermoelastic properties, shown in Fig. 11. The reference mesh selected for convergence analysis is the 1100 L9 + 4 B4.
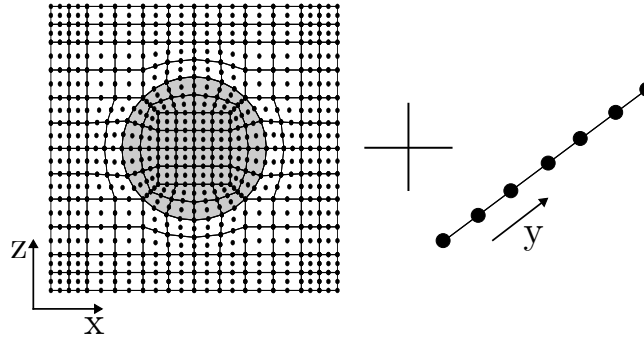

Figure 10 Discretization for the square-packed RVE with 176 L9 elements for the cross-section and 2 B4 elements along y-direction.

For the local stress analysis, two distinct load cases, derived from [43], were considered:

- A strain-free condition with a θ of 100 K.

- A unitary strain along x-direction (ε_{xx}=1) and a θ of 100 K.

Figures 12 and 13 show the distribution of local σ_{xx} for both load cases. The results suggest an excellent agreement of numerical outcomes when compared with SwiftComp [53] [54] and CUF-MSG [43].
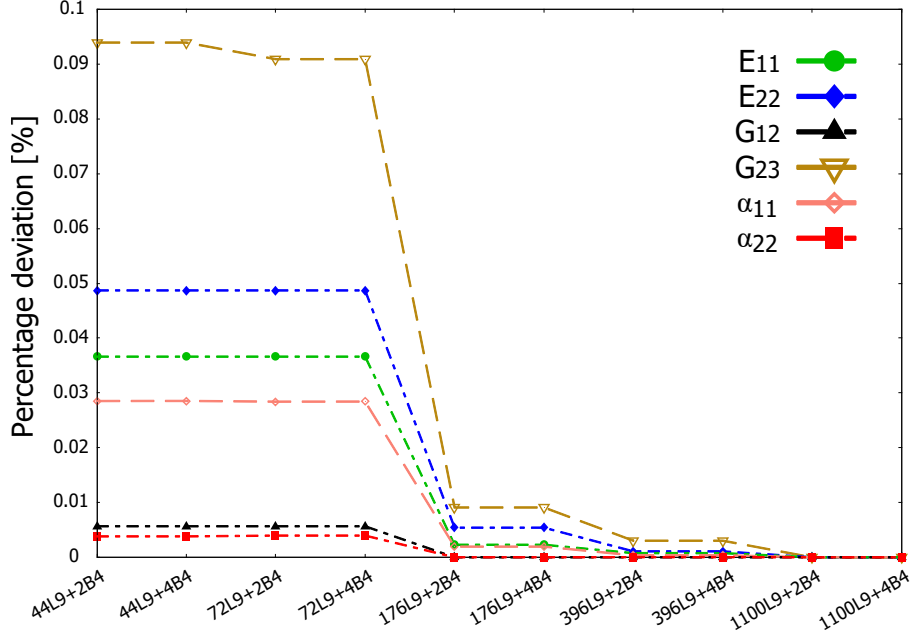
Figure 11 Convergence analysis on the thermoelastic properties for the square-packed RVE.
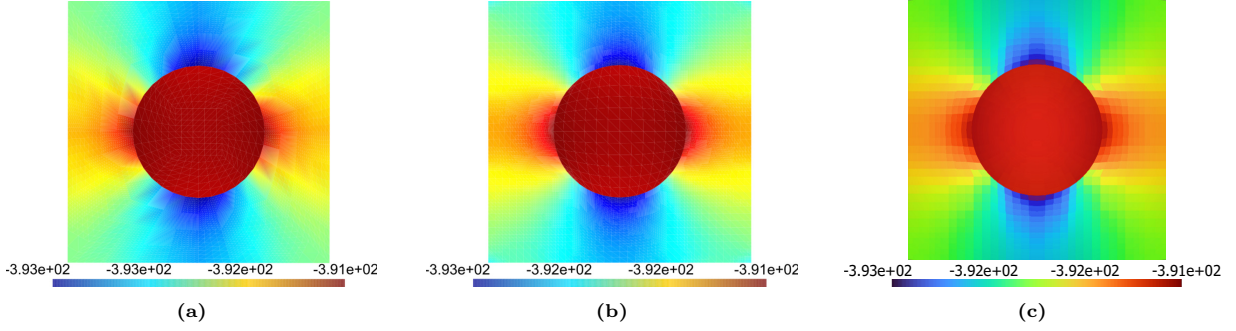

Figure 12 Distribution of local σ_{xx} (MPa) due to the application of a pure thermal load for (a) SwiftComp [53], (b) CUF-MSG [43], (c) CUF-MCM.

The maximum value of stress is 0.003% higher than the reference MSG considering the pure thermal case, whereas the maximum stress for the thermoelastic case is 1.1% lower than the CUF-MSG.

The second assessment investigates the void effect on the local stress field. A random distribution of fibers with a volume fraction of 47% characterizes the RVE, based on Pineda et al.'s work [55]. Table 1 contains the thermoelastic properties for the constituents derived from [38]. The T300 carbon fiber is modeled as an orthotropic material, and the epoxy resin matrix is associated with an isotropic behavior. The discretization consists of 277 L9 elements for the cross-section and 2 B4 elements along the y-direction, as shown in [44, 45, 46], with a number of 33068 DOF. Void volume fractions from 1 to 5% are considered, and the distribution over the matrix is illustrated in Fig. 14, where the adopted mesh is shown. Moreover, Table 9 presents the different load conditions for the current assessment.

The statistical analysis uses the parameters defined in Section 4, and Table 10 presents the statistical outcomes concerning the maximum stress over the matrix when applying the axial strain. Figure 15 shows boxplots of maximum local axial stress over the fiber for the random RVE.
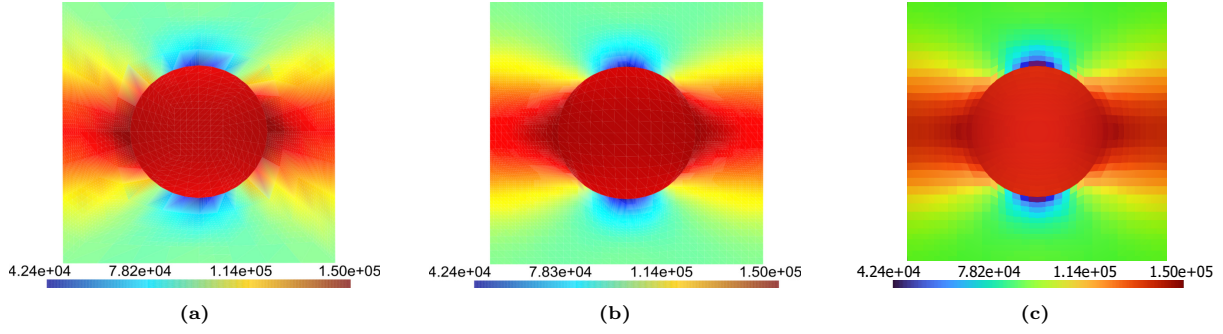
Figure 13 Distribution of local σ_{xx} (MPa) due to the application of a unitary strain along x-direction and thermal load for (a) SwiftComp [53], (b) CUF-MSG [43], (c) CUF-MCM.
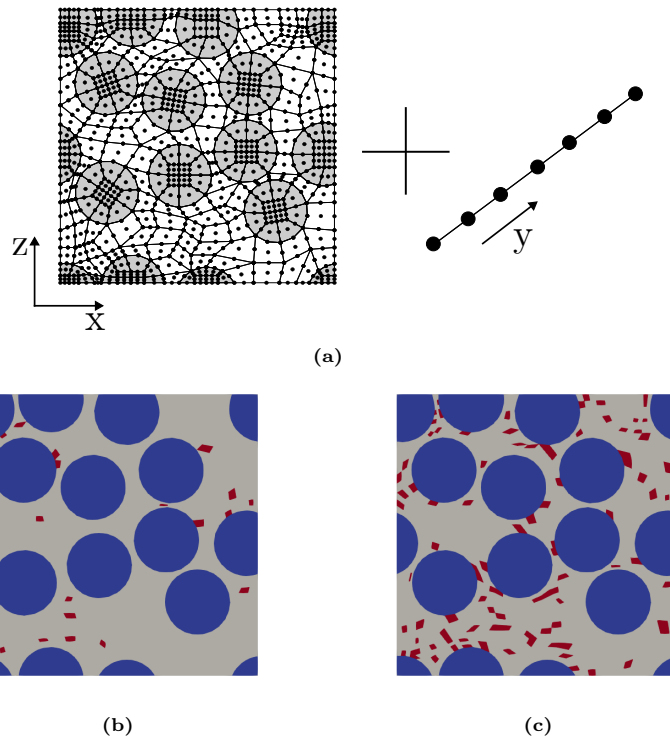

Figure 14 (a) Random RVE with 277 L9 elements for the cross-section and 2 B4 elements along y-direction, and an example of (b) 1% and (c) 5% of void volume fractions.

Table 9 Elastic boundary conditions applied on the RVE with random fibers and voids with $\theta = 50$ K.

	Strain	Void percentage	Subcases
Load case 1	$\varepsilon_{xx} = 5\ \mu\varepsilon$ Axial	1%, 2%, 3%, 4%, 5%	100
Load case 2	$\varepsilon_{xz} = 5\ \mu\varepsilon$ Shear	1%, 2%, 3%, 4%, 5%	100
Load case 3	$\varepsilon_{yz} = 5\ \mu\varepsilon$ Shear	no void*, 2%, 4%	100
Load case 4	No elastic strain	no void, 2%, 4%	1

*subcases not required; only one analysis is performed.

Table 10 Statistical parameters of stress (MPa) over the matrix for the random RVE when ε_{xx} is applied.

	$\bar{x}$	s	min	max	q_1	q_2	q_3	Voids [%]
	96.181	6.305	83.421	107.701	89.866	97.296	100.668	1
	101.128	6.342	88.044	119.365	97.210	100.871	104.244	2
σ_{xx}^{max}	103.464	6.573	89.892	126.526	99.566	102.417	107.191	3
	107.198	6.343	93.865	125.660	103.074	107.044	110.748	4
	109.319	6.162	95.222	126.207	105.552	108.748	112.997	5
	30.753	2.770	24.680	36.458	28.384	31.293	32.717	1
	33.319	3.357	26.030	44.549	30.908	33.238	34.707	2
σ_{yy}^{max}	34.944	3.333	28.267	44.805	32.923	33.982	36.358	3
	36.336	3.636	29.100	47.079	33.874	35.382	38.061	4
	37.589	3.247	32.057	47.247	35.281	37.046	39.579	5
	25.848	3.279	20.402	34.989	22.926	25.576	28.556	1
	28.415	3.364	21.257	39.179	25.763	28.758	30.497	2
σ_{zz}^{max}	30.286	3.303	22.154	42.523	28.378	30.299	31.882	3
	31.726	3.732	24.483	41.589	29.212	31.232	33.711	4
	32.893	3.031	28.282	43.013	30.474	32.797	34.958	5
	17.046	0.381	16.483	18.294	16.764	16.953	17.246	1
	17.229	0.493	16.471	19.198	16.810	17.188	17.511	2
σ_{xz}^{max}	17.329	0.647	16.198	18.979	16.850	17.220	17.681	3
	17.442	0.606	16.051	20.070	17.025	17.404	17.819	4
	17.673	0.640	16.326	19.543	17.203	17.601	18.027	5
	2.958	0.620	2.030	5.112	2.499	2.800	3.228	1
	3.598	0.610	2.346	5.473	3.099	3.521	4.032	2
σ_{yz}^{max}	4.249	0.743	2.994	6.379	3.741	4.159	4.701	3
	4.686	0.789	3.125	7.206	4.144	4.434	5.164	4
	5.293	1.000	3.672	8.377	4.629	5.157	5.809	5
	6.277	2.527	2.631	12.427	4.467	5.873	7.412	1
	7.637	2.617	3.432	15.776	5.541	6.990	9.937	2
σ_{xy}^{max}	8.793	2.393	4.342	17.075	6.825	9.072	10.029	3
	9.744	2.838	5.033	17.650	7.383	9.363	11.614	4
	10.715	2.937	4.960	23.504	8.820	10.175	11.809	5

The results related to applying the shear strain ε_{xz} are presented through the boxplots in Fig. 16. For load cases 3 and 4, Fig. 17a shows the distribution of σ_{yz} on the upper edge of the RVE for the thermoelastic simulation, whereas Figs. 17b and 17c show the statistical parameters of σ_{yz} over the fiber and the matrix. Fig. 18 reports the distribution of σ_{xx} with a strain-free condition on the upper edge and over the entire RVE.

The following comments stem from the analysis of the results:

- Voids induce higher stress peaks over the matrix when ε_{xx} is applied. Also, the fiber exhibits increased stress peaks and a larger variability range when the void volume fraction increases; however, the effect is more prominent over the matrix.

- The combination of shear strain ε_{xz} and the temperature leads to higher stresses over the matrix with increasing void volume fractions. On the other hand, shear stress along the x-direction over the fiber follows a decreasing distribution when the void percentage becomes higher. Voids significantly affect thermoelastic and pure thermal loading conditions.

- By observing the variation of shear stress on the upper edge of the RVE, the evolution along the x-direction shows minor differences between the case without void and with increased void content. More pronounced deviations are detected in the pure thermal load case.
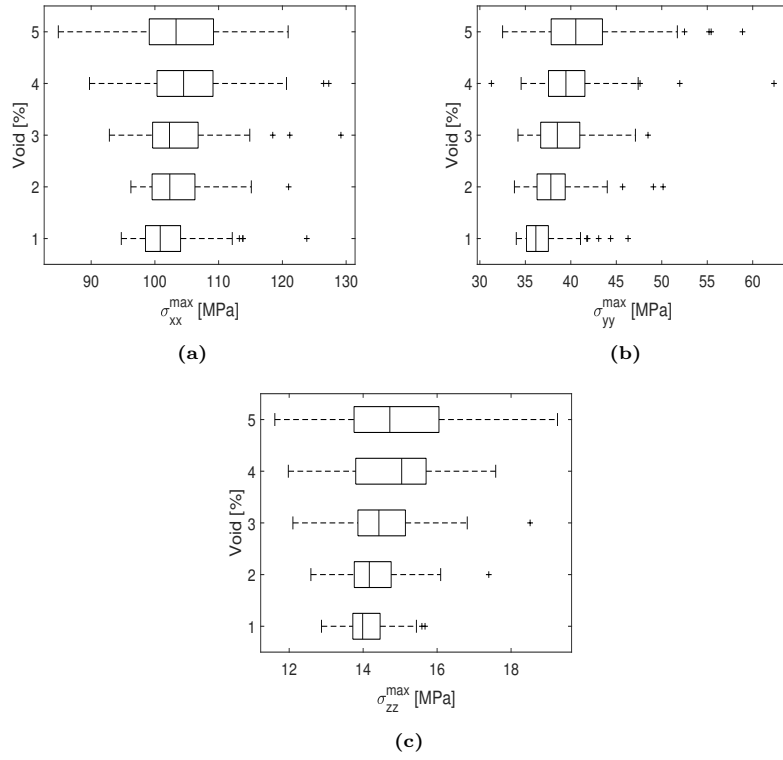
Figure 15 Boxplots of maximum (a) σ_{xx}, (b) σ_{yy}, and (c) σ_{zz} over the fiber for the random RVE when axial strain ε_{xx} is applied.
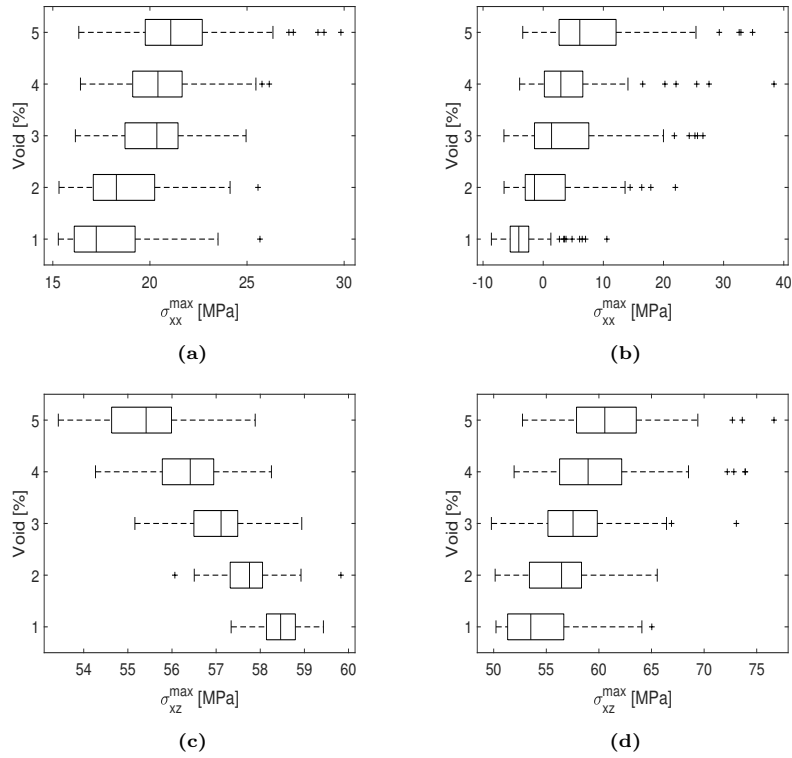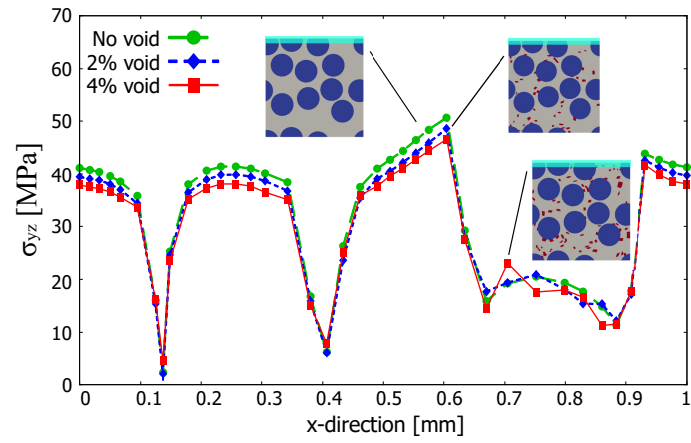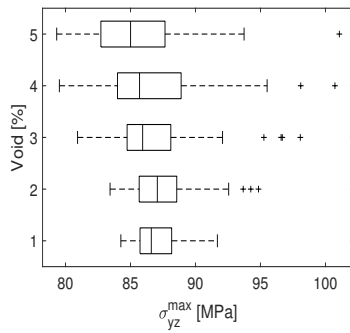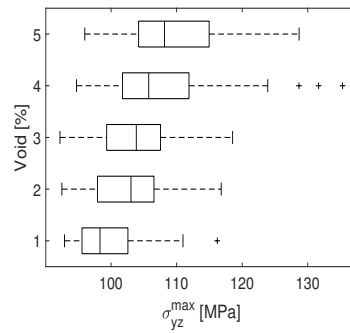

Figure 16 Boxplots of maximum σ_{xx} over the (a) the fiber and (b) the matrix, and boxplots of maximum σ_{xz} over (c) the fiber and (d) the matrix for the random RVE when shear strain ε_{xz} is applied.

19

(a)

(b)

(c)

Figure 17 Distribution of σ_{yz} on (a) the upper edge of the RVE and boxplots of maximum σ_{yz} over (b) the fiber and (c) the matrix, when shear strain ε_{yz} and θ are applied.
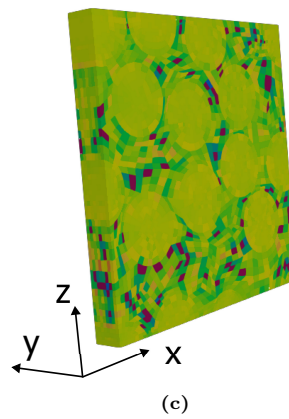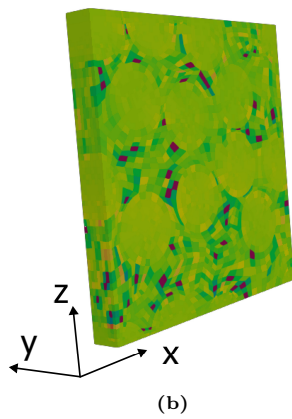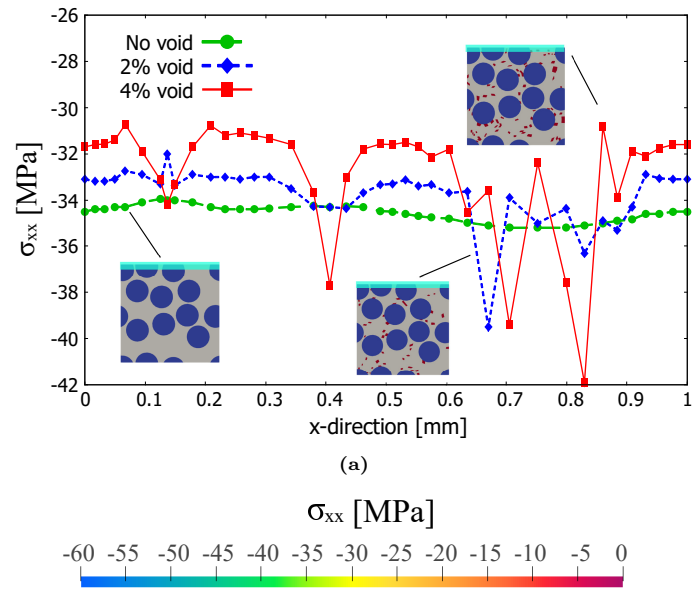
20

Figure 18 Distribution of σ_{xx} (MPa) with a strain-free condition on (a) the upper edge and over the entire RVE with (b) 2% and (c) 4% of void volume fraction.

6 Discussion

The initial numerical investigation demonstrates the robustness of the current CUF framework in determining the homogenized thermoelastic properties of pristine CFRP varying the fiber volume fractions. The results obtained from the CUF-MCM analysis, as shown in Fig. 5, exhibit a remarkable agreement with established methods, e.g., HFGMC [21], MSG-Solid model [38], CUF-MSG [43].

The second assessment thoroughly examines the capability of CUF micromechanics in determining the homogenized thermoelastic properties of composites with different void content. Initially, the analysis focuses on the pristine RVE, and the resulting homogenized properties are computed. The findings presented in Table 5 demonstrate a high level of agreement regarding longitudinal CTE. At the same time, slight differences are observed for the transversal CTE when compared to the 3D Abaqus model [39], probably due to differences in input material properties. The void content exerts a significant influence on the homogenized properties. The longitudinal CTE exhibits a decreasing trend, whereas a discernible increasing distribution is observed for the transversal CTE, as illustrated in Table 6. When comparing the CUF results with the reference [39], it is clear that a high void volume fraction leads to more significant differences, primarily due to the different modeling approaches employed for voids. Moreover, Table 7 indicates that the properties exhibit minor variations, as evidenced by the standard deviation values.

The final assessment aims to determine the local stress distribution within a square-packed pristine RVE domain. The reliability of the current framework is demonstrated under the application of a pure thermal load. A comparison between the current results and the MSG approach, as shown in Fig. 12, reveals a significant agreement. When considering the combined effect of mechanical strain and thermal loading, the local σ_{xx} distribution gets closer to the references. Although the stress peaks are slightly lower, as depicted in Fig. 13, the results still maintain a reasonable agreement regarding both stress distribution over the domain and the local stress peaks.

The presence of voids significantly affects the local stress peaks. Table 10 reveals that voids can increase the maximum stress within the matrix, particularly in the axial components. Additionally, higher void contents increase mean values and extend the range of stress variation within the fiber, as evidenced by the boxplots in Fig. 16. Applying shear strain alters the mean values with increasing void content. Specifically, the maximum σ_{xz} in the fiber exhibits a decreasing trend, as illustrated in Fig. 16, as shown in [46]. The void content also influences the variation of shear stress over the edge of the random RVE. Under a thermoelastic load, voids do not cause significant alterations in stress distribution over the edge of the RVE, as observed in Fig. 17. Notably, in the case of a pure thermal load, the stress exhibits more pronounced oscillations compared to the pristine architecture, as Fig. 18 suggests.

7 Conclusions

The present work has investigated the influence of void content on the micromechanical homogenized thermoelastic properties and the local responses of composites. The micromechanical model has been based on the Carrera Unified Formulation (CUF) and a Component Wise (CW) approach. Three Representative Volume Element (RVE) architectures have been considered, including an RVE with randomly placed fibers. Thermal and thermomechanical loads have been considered, and 3D distributions of stress fields have been obtained. Comparisons with data from the literature have been carried out. The numerical assessments have demonstrated that:

- The current micromechanical analysis based on CUF can predict the homogenized thermoelastic properties with good accuracy compared with well-established methods, e.g., the High-Fidelity Generalised Method of Cells (HFGMC) and the Mechanics of Structure Genome (MSG). It has been found that the relative variation between the current method and the MSG-based analysis, and HFGMC, produces differences in CTE values lower than 0.2% for each fiber volume fraction considered.

- The presence of voids has a significant impact on homogenized thermoelastic problems. Moreover, the statistical analysis has highlighted that the void content affects the range of variability of homogenized properties. Specifically, the longitudinal CTE for the RVE with V_f of 57% exhibits a decrease of 1.4% with void volume fraction ranging from 2 to 8%. In contrast, the CTE along the transverse direction demonstrates an increase of 4.0%. On the other hand, the small value of the standard deviation of CTE suggests that the final homogenized properties are less influenced by the distribution of voids throughout the matrix.

- CUF-MCM enables retrieving the local 3D stress fields induced by a thermoelastic load using a 1D formulation. Maximum CUF-MCM stress in the case of pure thermal conditions matches the reference. Furthermore, the maximum stress is lower by 1.1% compared to the benchmark for the thermoelastic load case.

- Voids influence the distribution of stress over the fiber and the matrix of the RVE. The matrix is the constituent mostly affected by voids since the maximum stress value tends to increase with higher void content. Examining the random RVE under axial strain ε_{xx}, the increased void content from 1 to 5% leads to a 13.5% variation of σ_{xx} over the matrix. However, σ_{xx} over the fiber has a more limited increase of about 2.9%. Similar variations are evident when the RVE is subjected to ε_{yz}. Specifically, the mean σ_{yz} exhibits an increase of 11.1% over the matrix and an increment of 2.4% over the fiber.

- The presence of voids leads to decreased shear stress over the fiber when ε_{xz} is applied since the maximum σ_{xz} decreases by 5.2% with 1 to 5% of void volume fraction. Conversely, the matrix exhibits a 10.9% rise in σ_{xz} with increasing void content in the same load case.

23

- Increments in void volume fractions influence stress distributions along the cross-section in thermoelastic and pure thermal load cases. For thermoelastic load cases, the RVE with 4% void content has a σ_{yz} distribution along the upper edge that is, on average, 3.2% lower than that of the pristine architecture. Furthermore, applying a pure thermal load to a 4% void RVE leads to a σ_{xx} distribution along the upper edge 5.1% higher, on average, than the RVE without defects.

Future research will include the impact of voids on a multiscale level, thus involving examining how the behavior of a material point interacts with a lower scale through explicit heterogeneous definitions via homogenization while also accounting for crack nucleation and propagation at the microscale level. Additionally, the research will explore the explicit modeling of voids and developing Convolutional Neural Network (CNN) models for predicting the homogenized elastic properties of fiber-reinforced composites.

References

[1] M. Mehdikhani, L. Gorbatikh, I. Verpoest, and S. V. Lomov. Voids in fiber-reinforced polymer composites: A review on their formation, characteristics, and effects on mechanical performance. *Journal of Composite Materials*, 53(12):1579–1669, 2019.

[2] J. E. Little, X. Yuan, and M. I. Jones. Characterisation of voids in fibre reinforced composite materials. *NDT & E International*, 46:122–127, 2012.

[3] ASTM International. Standard Test Methods for Void Content of Reinforced Plastics, 2016. ASTM Standard D2734-16.

[4] ASTM International. Standard Test Methods for Constituent Content of Composite Materials, 2009. ASTM Standard D3171-09.

[5] Y. Nikishkov, L. Airoldi, and A. Makeev. Measurement of voids in composites by X-ray Computed Tomography. *Composites Science and Technology*, 89:89–97, 2013.

[6] Q. Sun, G. M. Rizvi, C. T. Bellehumeur, and P. Gu. Effect of processing conditions on the bonding quality of FDM polymer filaments. *Rapid Prototyping Journal*, 14:72–80, 03 2008.

[7] B. Liao, H. Yang, B. Ye, and L. Xi. Microscopic void distribution of 3D printed polymer composites with different printing direction. *Materials Letters*, 341:134236, 2023.

[8] Q. He, H. Wang, K. Fu, and L. Ye. 3D printed continuous CF/PA6 composites: Effect of microscopic voids on mechanical performance. *Composites Science and Technology*, 191:108077, 2020.

[9] H. Jeong. Effects of Voids on the Mechanical Strength and Ultrasonic Attenuation of Laminated Composites. *Journal of Composite Materials*, 31(3):276–292, 1997.

[10] S. F. M. de Almeida and Z. d. S. N. Neto. Effect of void content on the strength of composite laminates. *Composite Structures*, 28(2):139–148, 1994.

[11] K. J. Bowles and S. Frimpong. Void Effects on the Interlaminar Shear Strength of Unidirectional Graphite-Fiber-Reinforced Composites. *Journal of Composite Materials*, 26(10):1487–1509, 1992.

[12] L. Maragoni, P. A. Carraro, and M. Quaresimin. Prediction of fatigue life to crack initiation in unidirectional plies containing voids. *Composites Part A: Applied Science and Manufacturing*, 127:105638, 2019.

[13] P. Olivier, J. P. Cottu, and B. Ferret. Effects of cure cycle pressure and voids on some mechanical properties of carbon/epoxy laminates. *Composites*, 26(7):509–515, 1995.

[14] L. Liu, B.-M. Zhang, D.-F. Wang, and Z.-J. Wu. Effects of cure cycles on void content and mechanical properties of composite laminates. *Composite Structures*, 73(3):303–309, 2006.

[15] L. Maragoni, P. A. Carraro, and M. Quaresimin. Effect of voids on the crack formation in a [45/-45/0]s laminate under cyclic axial tension. *Composites Part A: Applied Science and Manufacturing*, 91:493–500, 2016. CompTest 2015.

[16] A. E. Scott, I. Sinclair, S. M. Spearing, M. N. Mavrogordato, and W. Hepples. Influence of voids on damage mechanisms in carbon/epoxy composites determined via high resolution computed tomography. *Composites Science and Technology*, 90:147–153, 2014.

[17] S. Oshima, R. Higuchi, and S. Kobayashi. Experimental characterization of cracking behavior initiating from microdefects in cross-ply CFRP laminates. *Engineering Fracture Mechanics*, 281:109116, 2023.

[18] J. Aboudi. Micromechanical Analysis of Composites by the Method of Cells. *Applied Mechanics Reviews*, 42(7):193–221, 07 1989.

[19] M. Paley and J. Aboudi. Micromechanical analysis of composites by the generalized cells model. *Mechanics of Materials*, 14(2):127–139, 1992.

[20] J. Dai, E. J. Pineda, B. A. Bednarcyk, J. Singh, and N. Yamamoto. Micromechanics-based simulation of B4C-TiB2 composite fracture under tensile load. *Journal of the European Ceramic Society*, 42(14):6364–6378, 2022.

[21] J. Aboudi, M.-J. Pindera, and S. Arnold. High-Fidelity Generalization Method of Cells for Inelastic Periodic Multiphase Materials. 04 2002.

[22] C. T. Sun and R. S. Vaidya. Prediction of composite properties from a representative volume element. *Composites Science and Technology*, 56(2):171–179, 1996.

[23] S. Li and E. Sitnikova. *Representative Volume Elements and Unit Cells — Concepts, Theory, Applications and Implementation*. 11 2019.

[24] I. M. Gitman, H. Askes, and L. J. Sluys. Representative volume: Existence and size determination. *Engineering Fracture Mechanics*, 74(16):2518–2534, 2007.

[25] S. L. Omairey, P. D. Dunning, and S. Sriramula. Development of an ABAQUS plugin tool for periodic RVE homogenisation. *Engineering with Computers*, 35:567–577, 2019.

[26] Y. Wenbin. A unified theory for constitutive modeling of composites. *Journal of Mechanics of Materials and Structures*, 11:379–411, 08 2016.

[27] V. L. Berdichevskii. Variational-asymptotic method of constructing a theory of shells: PMM vol. 43, no.4, 1979, pp. 664–687. *Journal of Applied Mathematics and Mechanics*, 43(4):711–736, 1979.

[28] E. J. Barbero. *Finite Element Analysis of Composite Materials using Abaqus®*. CRC press, 2013.

[29] L. Yang, X. Liu, Z. Wu, and R. Wang. Effects of triangle-shape fiber on the transverse mechanical properties of unidirectional carbon fiber reinforced plastics. *Composite Structures*, 152:617–625, 2016.

[30] C. González and J. LLorca. Mechanical behavior of unidirectional fiber-reinforced polymers under transverse compression: Microscopic mechanisms and modeling. *Composites Science and Technology*, 67(13):2795–2806, 2007.

[31] J. Chevalier, P. P. Camanho, F. Lani, and T. Pardoen. Multi-scale characterization and modelling of the transverse compression response of unidirectional carbon fiber reinforced epoxy. *Composite Structures*, 209:160–176, 2019.

[32] J. He, X. Cui, J. Lua, and L. Liu. Interplay of manufacturing-induced thermal residual stresses and microvoids in damage and failure of fiber-reinforced composites. *International Journal of Mechanical Sciences*, 242:108000, 2023.

[33] J. Dong and N. Huo. A two-scale method for predicting the mechanical properties of 3D braided composites with internal defects. *Composite Structures*, 152:1–10, 2016.

[34] T. Huang and Y. Gong. A multiscale analysis for predicting the elastic properties of 3D woven composites containing void defects. *Composite Structures*, 185:401–410, 2018.

[35] H. Jiang, Y. Ren, Z. Liu, and S. Zhang. Microscale finite element analysis for predicting effects of air voids on mechanical properties of single fiber bundle in composites. *Journal of Materials Science*, 54, 01 2019.

[36] E. J. Pineda, B. A. Bednarcyk, T. M. Ricks, B. Farrokh, and W. Jackson. Multiscale failure analysis of a 3D woven composite containing manufacturing induced voids and disbonds. *Composites Part A: Applied Science and Manufacturing*, 156:106844, 2022.

[37] D. Ashouri Vajari, C. Gonzalez, J. Llorca, and B. N. Legarth. A numerical study of the influence of microvoids in the transverse mechanical response of unidirectional composites. *Composites Science and Technology*, 97:46–54, 2014.

[38] X. Liu, W. Yu, F. Gasco, and J. Goodsell. A unified approach for thermoelastic constitutive modeling of composite structures. *Composites Part B: Engineering*, 172:649–659, 2019.

[39] K. Wei, J. Li, H.-B. Shi, and M. Tang. Numerical evaluation on the influence of void defects and interphase on the thermal expansion coefficients of three-dimensional woven carbon/carbon composites. *Composite Interfaces*, 27(9):873–892, 2020.

[40] E. Carrera, M. Cinefra, M. Petrolo, and E. Zappino. *Finite Element Analysis of Structures Through Unified Formulation*. Wiley, New York, 2014.

[41] I. Kaleel, M. Petrolo, E. Carrera, and A. M. Waas. Computationally Efficient Concurrent Multiscale Framework for the Linear Analysis of Composite Structures. *AIAA Journal*, 57(9):4019–4028, 2019.

[42] I. Kaleel, M. Petrolo, E. Carrera, and A. M. Waas. Computationally Efficient Concurrent Multiscale Framework for the Nonlinear Analysis of Composite Structures. *AIAA Journal*, 57(9):4029–4041, 2019.

[43] A. R. Sánchez-Majano, R. Masia, A. Pagani, and E. Carrera. Microscale thermo-elastic analysis of composite materials by high-order geometrically accurate finite elements. *Composite Structures*, 300:116105, 2022.

[44] E. Carrera, M. Petrolo, M. H. Nagaraj, and M. Delicata. Evaluation of the influence of voids on 3D representative volume elements of fiber-reinforced polymer composites using CUF micromechanics. *Composite Structures*, 254:112833, 2020.

[45] M. H. Nagaraj, I. Kaleel, E. Carrera, and M. Petrolo. Elastoplastic Micromechanical Analysis of Fiber-Reinforced Composites with Defects. *Aerotecnica Missili & Spazio*, 101(1):53–59, November 2021.

[46] M. Petrolo, A. Pagani, M. Trombini, and E. Carrera. Voids effect on micromechanical response of elastoplastic fiber-reinforced polymer composites using 1D higher-order theories. *Mechanics of Materials*, 184:104747, 2023.

[47] Z. Xia, Y. Zhang, and F. Ellyin. A unified periodical boundary conditions for representative volume elements of composites and applications. *International Journal of Solids and Structures*, 40(8):1907–1921, 2003.

[48] C. T. Sun and R. S. Vaidya. Prediction of composite properties from a representative volume element. *Composites Science and Technology*, 56:171–179, 1996.

[49] E. Langford. Quartiles in Elementary Statistics. *Journal of Statistics Education*, 14(3), 2006.

[50] W. Haynes. *Probability Distributions*, pages 1752–1754. Springer New York, New York, NY, 2013.

[51] R. Mcgill, J. W. Tukey, and W. A. Larsen. Variations of Box Plots. *The American Statistician*, 32(1):12–16, 1978.

[52] S. Nemat-Nasser and M. Hori. *Micromechanics: overall properties of heterogeneous materials*. Elsevier, 2013.

[53] W. Yu and X. Liu. SwiftComp, January 2017.

[54] W. Yu and T. Tang. A variational asymptotic micromechanics model for predicting thermoelastic properties of heterogeneous materials. *International Journal of Solids and Structures*, 44(22):7510–7525, 2007.

[55] E. J. Pineda, B. A. Bednarcyk, A. M. Waas, and S. M. Arnold. Progressive failure of a unidirectional fiber-reinforced composite using the method of cells: Discretization objective computational results. *International Journal of Solids and Structures*, 50(9):1203–1216, 2013.